Stopped Light at High Storage Efficiency in a Pr^{3+} : Y_2SiO_5 Crystal

Daniel Schraft,[*] Marcel Hain, Nikolaus Lorenz, and Thomas Halfmann[†]

Institut für Angewandte Physik, Technische Universität Darmstadt, Hochschulstr. 6, 64289 Darmstadt, Germany
(Received 31 October 2015; published 17 February 2016)

We demonstrate efficient storage and retrieval of light pulses by electromagnetically induced transparency (EIT) in a Pr^{3+} : Y_2SiO_5 crystal. Using a ring-type multipass configuration, we increase the optical depth (OD) of the medium up to a factor of 16 towards $OD \approx 96$. Combining the large optical depth with optimized conditions for EIT, we reach a light storage efficiency of $(76.3 \pm 3.5)\%$. In addition, we perform extended systematic measurements of the storage efficiency versus optical depth, control Rabi frequency, and probe pulse duration. The data confirm the theoretically expected behavior of an EIT-driven solid-state memory.

Introduction.—Storage of coherent optical information in quantum systems is a central requirement of optical quantum information technology, e.g., in deterministic single photon sources, quantum networks, or quantum repeaters [1,2]. In particular, specific atomlike solids have attracted attention as potential quantum memories. Examples for such solids, which combine advantages of free atoms in the gas phase (i.e., spectrally narrow transitions and long decoherence times) and solids (i.e., scalability, capability of being integrated in larger architectures, and easy handling) are quantum dots, color centers, or dopant ions in solids, e.g., rare-earth ion-doped crystals. The latter were already known for decades from classical optical data storage [3,4]. A variety of protocols for quantum memory applications have been implemented so far in atomic gases or specific rare-earth ion-doped solids, e.g., gradient echo memories, off-resonant Raman-type excitations, atomic frequency combs, or electromagnetically induced transparency (EIT) [5,6].

The most important properties of any type of memory or storage protocol are the achievable storage time, storage capacity, and storage efficiency (also related to the fidelity). With regard to the storage capacity and storage time, in previous work, we combined EIT light storage with multiplexing in frequency and/or propagation angle [7], and demonstrated storage of spatially multiplexed information (i.e., images) in a rare-earth ion-doped crystal, reaching storage times up to one minute [8]. This set a new benchmark for any type of coherent storage protocols in quantum systems. However, the storage efficiency η, defined as the ratio of the output signal pulse energy E_{out} and the input probe pulse energy E_{in}, i.e., the net efficiency of the EIT storage protocol itself, without losses due to imperfections in the optical setup, in all these investigations was below 1%. This was mainly due to nonoptimized pulse parameters, which led to improper EIT conditions. However, even at optimized pulse parameters, there is always a maximal efficiency limit set by the finite optical depth (OD) of the medium, defined by $OD = n\sigma L$, with the density n, absorption cross section σ, and the medium length L [9–11].

The largest EIT storage efficiency, so far, was achieved in a spatially confined, cigar-shaped cloud of cold atoms from a magneto-optical trap (MOT), providing optical depths up to $OD = 156$, reaching maximal efficiencies of 71% in forward retrieval configuration (i.e., the signal pulse retrieved in the same direction as the input probe pulse was stored, realized by copropagating control write and read pulses) and 78% in backward retrieval configuration (i.e., the signal pulse retrieved in the opposite direction as the input probe pulse was stored, realized by counter-propagating control write and read pulses) [12]. The latter configuration is known to yield higher efficiencies [9–11]. In principle, it would be possible to further increase the EIT storage efficiency via even higher optical depth in cold atom setups, e.g., by scaling the experiment up with a MOT of larger dimensions [13]. In a different approach towards large optical depth, cold atoms were loaded into a hollow-core optical fiber, providing strong spatial confinement and long interaction length, yielding optical depth beyond 1000 [14]. Another idea is to build a cavity setup around the storage medium to enhance the optical depth of the system [10,15,16]. However, in rare-earth ion-doped solids, this idea is difficult to implement. Large inhomogeneous broadenings in such media require optical preparation by spectral hole burning, which results in slow light effects and narrowing of the cavity bandwidth [17]. This makes it impossible to feed probe and control pulses at different frequencies into the cavity. Implementation of a cavity for the probe pulse alone, with the control pulse intersecting at a small angle would require a quite long cavity with active stabilization, i.e., an already complicated setup [18]. Thus, there is no demonstration yet of large EIT light storage efficiencies in a solid medium. In principle, solid-state memories should offer simple ways to achieve large OD by increasing the medium length L or the density n, e.g., the dopant concentration in a rare-earth doped crystal. However, increasing the dopant concentration usually quickly leads to severe problems, e.g., stress-induced broadening of lines and reduction of coherence

lifetimes [19,20]. Increasing the medium length L is also only possible within certain limits, as the medium is typically embedded in compact setups to control the optically driven coherences or prepare the system, e.g., by static and dynamic magnetic fields. Increasing the sample dimensions typically leads to an increase in the inhomogeneity of the control setups and, hence, errors in the applied control strategies and storage protocols. Thus, typical samples of rare-earth doped solids for memory applications have dimensions of a few mm in all directions, which limits the achievable OD to values below 10. This theoretically limits EIT light storage efficiency to values below 50%. A straightforward way to increase the optical depth of a sample is to use it in a multipass configuration, e.g., by retroreflecting the probe pulse. Such a setup effectively increases the length of the medium $L_{\text{eff}} = NL$, with the number of passes N, thus, leading to $\text{OD} = n\sigma NL$. This is possible for EIT light storage, provided the extra optical path lengths in the multipass setup outside of the medium are small compared to the pulse lengths of the probe and control pulses. For typical narrowband pulses with durations far beyond a few nanoseconds, this is usually guaranteed.

The goal is to set up a multipass configuration permitting $N > 10$ passes, without variations in the overlap of focused probe beams and the control beam from pass to pass, and with the possibility to systematically vary the number of passes. The setup has to be built around a small crystal and be embedded in an already existing compact control setup, with optical apertures of a few millimeters only. Below, we report on a multipass geometry in an EIT light storage setup with a rare-earth ion-doped crystal as memory. The setup enables a variable number of passes, reaching optical depths up to $\text{OD} \approx 96$ for $N = 16$ passes and light storage efficiencies in forward retrieval of $(76.3 \pm 3.5)\%$ for $N = 14$ passes. This ties the current EIT light storage record in cold atoms of $(78 \pm 3)\%$ [12] and sets a new benchmark for EIT light storage efficiency in solid-state memories.

Theoretical background.—Light storage by EIT uses a strong control write pulse, tuned to the transition between the states $|2\rangle$ and $|3\rangle$ of a Λ-type system (see Fig. 1), which are initially not populated. The coherent interaction with the control pulse modifies the optical properties of the quantum system. In particular, the medium becomes transparent for a probe pulse (which represents an input data bit) tuned to the transition between a populated ground state $|1\rangle$ and the excited state $|3\rangle$. In addition, the group velocity v_{gr} of the probe pulse, is significantly reduced and the probe pulse is, thus, compressed in the medium. By reducing the control pulse intensity adiabatically, the "slow light" probe pulse is "stopped" and converted into an atomic superposition ρ_{12} of the quantum states $|1\rangle$ and $|2\rangle$ along the light propagation path z. This establishes a spin wave $S(z)$ of spatially distributed atomic coherences $\rho_{12}(z)$ in the medium, which contains all information of the incoming probe pulse [5]. The spin wave can be read out by applying
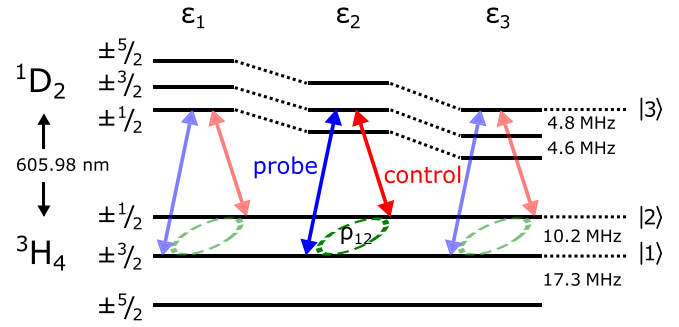
FIG. 1. Coupling scheme for three frequency ensembles ϵ_i of Pr^{3+} ions in a Y_2SiO_5 host lattice in the inhomogeneous line of the optical transition.

a control read pulse to beat with the atomic coherences and generate a signal pulse, i.e., a time inverted copy of the input probe pulse.

As Gorshkov *et al.* theoretically showed [9–11], the maximal storage and retrieval efficiency of EIT light storage is limited by the optical depth of the medium only—provided the temporal intensity profiles and frequencies of the driving pulses are matched to enable optimal EIT conditions. This can be understood by considering the conditions for EIT and slow light [5]: we would find perfect EIT light storage, i.e., 100% storage efficiency, if, on one hand, the probe pulse to be stored is compressed entirely into the medium. Thus, the compressed probe pulse length L_p must be shorter than the medium length L, i.e., $L_p \approx 3 v_{\text{gr}} \tau_p \lesssim L$, with the group velocity v_{gr}, and the probe pulse duration τ_p (FWHM, assuming a Gaussian temporal profile). On the other hand, the spectral EIT bandwidth Γ_{EIT} must be sufficiently large to fully cover the probe pulse bandwidth $\Delta\omega_p$, i.e., $\Gamma_{\text{EIT}} \gg \Delta\omega_p = 2\pi\Delta\nu_p = 4\ln 2/\tau_p$. From the linear susceptibility and the amplitude transfer function for EIT [5], assuming a resonant control pulse in the Λ system, we get the bandwidth (FWHM) of the EIT window close to the probe resonance as

$$\Gamma_{\text{EIT}} = \frac{\Omega_c^2}{\gamma_{31}} \frac{\sqrt{\ln 2}}{\sqrt{\text{OD}}}, \tag{1}$$

with the control Rabi frequency Ω_c and the coherence decay rate γ_{31} at the probe transition. Hence, the EIT bandwidth decreases with increasing OD. On the other hand, the group velocity for the probe pulse is given by $v_{\text{gr}} = c/(1 + n_{\text{gr}})$, with $n_{\text{gr}} = c\gamma_{31}\text{OD}/(\Omega_c^2 L)$. Hence, the pulse compression becomes stronger with larger optical depth. Combining the two conditions for sufficiently large EIT bandwidth and sufficiently large pulse compression, we get

$$12\sqrt{\ln 2}\sqrt{\text{OD}} \ll \frac{3\Omega_c^2 \tau_p}{\gamma_{31}} \leq \text{OD}. \tag{2}$$

In a further simplified version, this can be approximately written as $\sqrt{\text{OD}} \ll \text{OD}$. Obviously, the latter condition for

efficient EIT light storage can be fulfilled at large optical depth only.

Experimental setup.—We conduct the experiment in Praseodymium Pr^{3+} ions doped into an Yttrium orthosilicate crystal (in the following, termed PrYSO). The length of the sample is $L = 3$ mm, the dopant concentration is 0.05%. We determine the optical depth in a single pass to be OD ≈ 6. The crystal is placed inside a liquid helium cryostat (type ST-100, Janis Research Co.) to keep the temperature below 4 K and reduce interactions with phonons. PrYSO exhibits three hyperfine levels in the $^3H_4$ ground state manifold and in the optically excited state $^1D_2$ (see Fig. 1). The frequency differences between the hyperfine levels are in the range of 10 MHz. The optical transition at 605.98 nm is inhomogeneously broadened to $\Gamma_{opt} \approx 7$ GHz. The hyperfine ground states in the $^3H_4$ manifold have a homogeneous linewidth below 1 kHz (leading to a decoherence time $T_2 \approx 500$ μs), inhomogeneous linewidth in the range of 30 kHz (leading to a dephasing time $T_{deph} \approx 10$ μs), and long population relaxation times T_1 up to the regime of one minute. A solid-state laser system [21] generates the required optical radiation for the experiment. The laser system is frequency stabilized by a Pound-Drever-Hall setup to a bandwidth below 100 kHz (FWHM) on a time scale of 100 ms. The laser output is split into beam lines for an optical preparation sequence prior to the EIT experiment, control pulse, and probe pulse for EIT light storage. Acousto-optical modulators enable full temporal control over all pulse intensities and frequencies. The preparation sequence is based on optical pumping to empty and repump hyperfine ground states of specific frequency ensembles in the inhomogeneous broadening of the optical transition (similarly shown in [22]). This provides Λ-type systems (see Fig. 1) with population in state $|1\rangle$, as required for EIT. To apply the maximal possible optical depth of the crystal, we shifted the repump pulse frequency compared to preparation sequences in previous experiments [22]. Thereby, we prepare three frequency ensembles ϵ_1, ϵ_2, ϵ_3 in the optical inhomogeneous bandwidth simultaneously. For each of these ensembles the excited state $|3\rangle$ of the Λ-type systems is a different hyperfine state of $^1D_2$. For EIT light storage, a control write pulse converts the probe pulse to a spin wave of atomic coherences between hyperfine states $|1\rangle$ and $|2\rangle$. For retrieval, interaction of the spin wave with a control read pulse generates a signal pulse. In our specific experiment, we set the time delay between the control write and control read pulses (i.e., the storage time) to $\Delta t = 2$ μs in order to stay well below the dephasing and decoherence times. For detection and determination of the storage efficiency η, a first photodiode (PDA 10A-EC, Thorlabs Inc.) measures the input probe pulse energy E_{in} and a second photodiode (2051-FS, New Focus) measures the output signal pulse energy E_{out}. The photodiodes are calibrated with respect to each other,
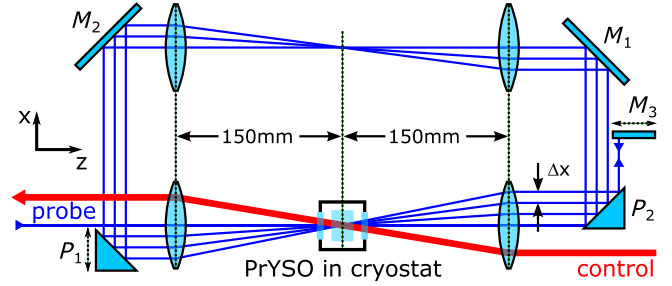
FIG. 2. Schematic of the multipass ring geometry for a variable number of passes of the probe beam through the PrYSO memory in a cryostat, with reflective prisms P_1, P_2, mirrors M_1, M_2, M_3, and two telescope systems in $4f$ configurations. Figure shows the beam path for $N = 8$ passes as an example. We neglect all other components of the extended optical and laser setup for the light storage experiment. A lateral shift of prism P_1 in x direction changes the spatial distance Δx between two passes, the total number of round-trips is varied by shifting mirror M_3 in z direction.

signals are recorded using an oscilloscope (TDS 2014B, Tektronix). Typical laser beam parameters for the probe (p) and control (c) pulses in the light storage sequence are powers $P_p \leq 350$ μW and $P_c \leq 280$ mW, pulse durations $\tau_p = 1 - 60$ μs and $\tau_c = 200$ μs, diameters (FWHM) in the interaction region $d_p = 170$ μm and $d_c = 750$ μm, yielding peak Rabi frequencies up to $\Omega_p \approx 2\pi \times 90$ kHz and $\Omega_c = 2\pi \times 470$ kHz. To increase the optical depth of the medium, we implemented a multipass setup for the probe beam, which is matched to the small aperture and tight geometrical constraints of the crystal with closely attached control setup, and also permits systematic measurements by variation of the number of passes by simple adjustment of a single optical element. Figure 2 shows a schematic of the relevant parts of the multipass setup, depicted for $N = 8$ passes through the PrYSO crystal. The setup resembles a ring, made of mirror elements P_1, P_2, M_1, M_2, and two telescope systems. The probe beam coupled into the ring is collimated with a diameter of 360 μm. The optical path in the ring is chosen such that, after each round-trip, the probe beam is laterally shifted by a small distance Δx. This already permits m passes, which are limited by the ratio of the prism dimensions and the probe beam diameter. After m passes, the probe beam is retroreflected by mirror M_3 and travels back another m passes, till it leaves the setup opposite to the initial input direction. The telescope systems in $4f$ configuration serve to focus the beam $N = 2m$ times into the interaction region, and to maintain the probe beam profile for each pass by relay imaging. The total number of passes can be varied by simply shifting the position of mirror M_3 in z direction with a translation stage. The distance Δx between two adjacent passes can be adjusted by shifting the prism P_1 in x direction. In our experiment, we achieved up to $N = 16$ passes. The overall transmission losses per pass, due to nonperfect optical components add up to approx. 13%.

These losses are not included in the definition of the storage efficiency. We note that, at pulse durations in the regime of 10 μs, the optical delays (i.e., optical path outside of the crystal) of roughly 4 ns per round-trip have a negligible effect on the storage process. The control beam propagates under a small angle of 1° with regard to the incoming probe beam and passes only once through the crystal. Therefore, we note that the first half of probe passes (before M_3) is stored with an almost counter-propagating control beam, while the second half of probe passes (after M_3) is stored with an almost copropagating control beam. Nevertheless, each temporal slice of the probe beam is retrieved with the control read beam under the same angle as it was stored before with the control write beam. Thus, the setup uses the standard EIT forward read configuration.

Experimental results.—In order to experimentally determine the dependence of the maximal light storage efficiency η upon the optical depth OD, we proceed as follows: we vary the number of passes in the multipass setup from a single pass $N = 1$ up to $N = 16$. For each number of passes N, in a first step, we perform light storage measurements and systematically vary the control pulse power P_c, i.e., control pulse Rabi frequency Ω_c, and the probe pulse duration τ_p of simple rectangular pulses to match Eq. (2). By this measurement, we, on one hand, adjust the EIT bandwidth Γ_{EIT} to the probe bandwidth $\Delta\omega_p$, and, on the other hand, we match the probe pulse length L_p to the effective length of the medium $L_{\mathrm{eff}} = NL$.

Figure 3(a) shows the variation of the light storage efficiency η for a single pass through the crystal versus control pulse power P_c and probe pulse duration τ_p. The region of largest efficiency exhibits a hyperbola, determined by the relation $P_c\tau_p \propto \Omega_c^2\tau_p = \mathrm{const}$, confirming Eq. (2). We note that, for larger probe pulse durations (and, hence, small control Rabi frequencies to provide an optimized combination), the storage efficiency slowly drops. In a three level system without any inhomogeneous
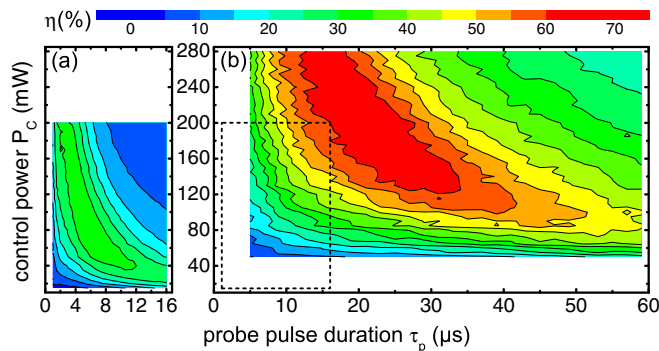
FIG. 3.   EIT light storage efficiency η versus control power P_c and probe pulse duration τ_p of a rectangular pulse for a single pass ($N = 1$) (a), and $N = 10$ passes (b) of the probe beam. Please note that the parameter ranges of P_c and τ_p in (a) and (b) are quite different. The dotted square in (b) indicates the parameter range of (a).
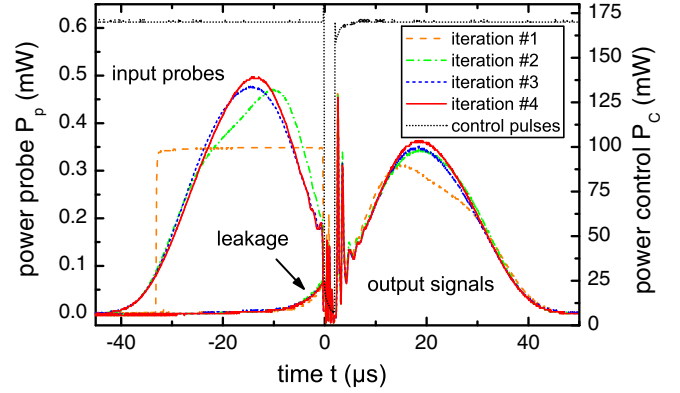
FIG. 4.   Iterative procedure for optimizing the temporal probe intensity profile for maximal light storage efficiency. Power of input probe pulses and output signals versus time, for $N = 14$ passes, a storage time of 2 μs, and fixed control pulse shape with control power $P_c = 170$ mW. For a rectangular probe pulse shape with a duration of $\tau_p = 33$ μs, we start with a storage efficiency of 70.3%. After four iterations the temporal intensity profile of the probe pulse converges to a truncated Gaussian-like shape with a FWHM of 23.5 μs, reaching a storage efficiency of (76.3 ± 3.5)%.

broadenings, this is due to the fact that, at finite coherence decay rate γ_{21}, the residual absorption in the EIT window increases with decreasing control Rabi frequency. In PrYSO, the inhomogeneous broadenings of the prepared optical transition (≈ 500 kHz) and the hyperfine transition (≈ 30 kHz) lead to residual absorption in the EIT window, thus, limiting the storage efficiency at large probe pulse durations. The maximal storage efficiency in this single pass and for not optimized temporal pulse shapes yields 33.8%. Figure 3(b) depicts a similar measurement for $N = 10$ passes. As the OD increases, Eq. (2) is fulfilled better, the maximal storage efficiency is higher and reaches 67%. The comparison of Figs. 3(a) and 3(b) shows that the optimal combination of probe pulse duration and control power (i.e., control Rabi frequency) changes with optical depth, from ($P_c \approx 80$ mW; $\tau_p \approx 6$ μs) for $N = 1$ to ($P_c \approx 180$ mW; $\tau_p \approx 24$ μs) for $N = 10$. This is due to the fact that, at larger optical depth (e.g., in an effectively longer medium due to more passes), longer probe pulses can also be compressed into the medium. However, with an increase of the optical depth, the EIT bandwidth Γ_{EIT} is reduced. Larger control Rabi frequencies (i.e., larger control powers) are required for compensation.

In a second step, we vary the temporal intensity profile of the probe pulse to optimize the spin wave $S(z)$ resulting in maximal light storage efficiency [11] (see Fig. 4). To achieve this goal, we apply an iterative optimization procedure, developed and first implemented by Novikova *et al.* in cold atoms [23,24]. It starts from an arbitrary probe pulse shape in the first iteration and uses the retrieved signal pulse as probe pulse shape for the next iteration. For high OD, the optimized intensity profile of the probe pulse resembles a truncated Gaussian-like shape,

which, on one hand, has to be sufficiently short to minimize the leakage (i.e., part of the probe pulse which spatially does not fit into the storage medium). On the other hand, the probe still has to be sufficiently long and smooth to exhibit a bandwidth $\Delta\omega_p$ comparable to or smaller as the EIT bandwidth Γ_{EIT}. Figure 4 shows the optimization for $N = 14$, starting with a rectangular intensity profile of the probe pulse. After a few iterations, the optimization procedure converges to an optimal solution. We note that the fast oscillations in the signal pulse (i.e., temporally close to the fast rising edge of the control read pulse) could be due to residual diabatic couplings upon readout, generated by the fast switching of the control read pulse. We checked, experimentally, that the oscillations are considerably suppressed at slower switching of the control read pulse. After every iteration, we smooth these oscillations before we use it as the new input probe pulse shape. We repeat optimization steps one and two for different numbers of passes N through the crystal. Figure 5 (red solid squares) shows the measured maximal light storage efficiency η versus the number of passes N (i.e., the effective OD). Up to $N = 10$ passes, the efficiency increases with increasing OD. The experimental data confirm the theoretical expectation [11] very well (see black solid line in Fig. 5). However, for passes $N > 10$, the efficiency does not increase any more. This is mainly due to technical problems at larger numbers of passes, e.g., the probe beam profile passing through 14 optical interfaces per round-trip deteriorates more and more, and small vibrations lead to problems in overlap of control and probe beam and propagation of the probe beam through the ring. The total transmission T through the ring reduces with an increasing number of passes N, due to reflection losses at all optical components.

Nevertheless, for $N = 14$ passes, we get a maximal light storage efficiency of $(76.3 \pm 3.5)\%$ in forward retrieval configuration (see, also, Fig. 4). This is 5% higher than the best results obtained, so far, in EIT forward
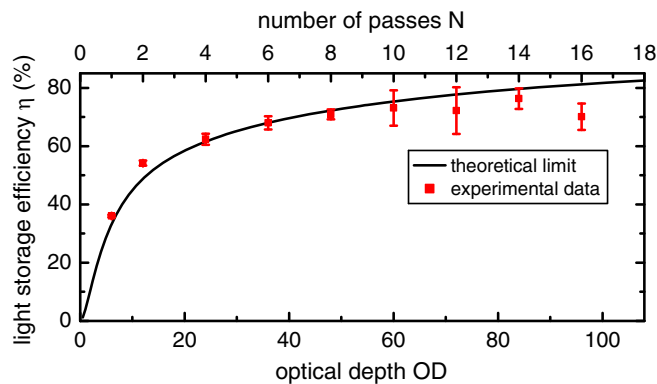
configuration, and reaches the previous record for backward configuration, both implemented in a cold atomic gas [12] and the, so far, largest light storage efficiency in a solid state memory. We note that, in principle, application of backward retrieval could further improve our results. However, backward retrieval is more difficult to implement for nonparallel probe and control beams, as the generated signal pulse leaves the medium in a different (i.e., neither collinear nor anticollinear) direction compared to the incoming probe pulse. Moreover, in a multipass setup where the probe pulse is stored in multiple individual portions with different angles relative to the control pulse, the individual parts of the signal pulse will not pass the setup in the same way.

Conclusion.—We presented systematic measurements of the light storage efficiency η in an EIT-driven solid-state memory, i.e., a rare-earth ion-doped crystal. In particular, we demonstrated the implementation of a multipass setup consisting of a ringlike arrangement, which also permits simple variation of the number of passes through the crystal, up to 16 passes. With this setup, we could increase the optical depth of our medium from OD ≈ 6 to OD ≈ 96, resulting in a significant increase of the storage efficiency. We further optimized the storage efficiency by systematic variation of control power (i.e., control Rabi frequency), probe pulse duration, and temporal probe intensity profile. With regard to the latter, we applied an iterative, experimental approach to provide optimized conditions for EIT light storage. We achieved a storage efficiency of $(76.3 \pm 3.5)\%$ at $N = 14$ passes in forward retrieval configuration, reaching the previous record in an EIT-driven memory of cold atoms [12], and setting a new benchmark for solid state memories. Our data agree well with theoretical calculations of the maximal possible storage efficiency, which is only limited by the optical depth of a medium. In addition, we presented systematic measurements of the EIT light storage efficiency versus the driving control power P_c (i.e., control Rabi frequency Ω_c) and probe pulse duration τ_p. This reveals maximal and almost constant efficiency for $P_c\tau_p \propto \Omega_c^2\tau_p = $ const, as expected from simple considerations of EIT bandwidth and pulse compression by EIT-driven slow light. Our investigations are meant as an important step forward towards the implementation of a coherently driven, all-solid state memory for photons, i.e., a basic component of any quantum information architecture.

FIG. 5. Maximal light storage efficiency η, experimental data (red solid squares) and theory (black solid line), versus number of passes N (i.e., optical depth OD).

*daniel.schraft@physik.tu-darmstadt.de
†http://www.iap.tu-darmstadt.de/nlq

[1] C. Simon *et al.*, Eur. Phys. J. D **58**, 1 (2010).

[2] A. I. Lvovsky, B. C. Sanders, and W. Tittel, Nat. Photonics **3**, 706 (2009).

[3] A. A. Kaplyanskii and R. M. Macfarlane, *Spectroscopy of Solids Containing Rare Earth Ions*, Modern Problems in Condensed Matter Sciences, Vol. 21 (Elsevier, New York, 1987).

[4] S. Kröll, E. Xu, R. Kachru, and D. Huestis, Springer Series on Wave Phenomena **9**, 342 (1990).

[5] M. Fleischhauer, A. Imamoglu, and J. P. Marangos, Rev. Mod. Phys. **77**, 633 (2005).

[6] J. P. Marangos and T. Halfmann, *Electromagnetically-Induced Transparency*, in Handbook of Optics Vol. IV (McGraw-Hill Professional, New York, 2009).

[7] G. Heinze, N. Rentzsch, and T. Halfmann, Phys. Rev. A **86**, 053837 (2012).

[8] G. Heinze, C. Hubrich, and T. Halfmann, Phys. Rev. Lett. **111**, 033601 (2013).

[9] A. V. Gorshkov, A. André, M. Fleischhauer, A. S. Sørensen, and M. D. Lukin, Phys. Rev. Lett. **98**, 123601 (2007).

[10] A. V. Gorshkov, A. André, M. D. Lukin, and A. S. Sørensen, Phys. Rev. A **76**, 033804 (2007).

[11] A. V. Gorshkov, A. André, M. D. Lukin, and A. S. Sørensen, Phys. Rev. A **76**, 033805 (2007).

[12] Y.-H. Chen, M.-J. Lee, I-C. Wang, S. Du, Y.-F. Chen, Y.-C. Chen, and I. A. Yu, Phys. Rev. Lett. **110**, 083601 (2013).

[13] Y.-F. Hsiao, H.-S. Chen, P.-J. Tsai, and Y.-C. Chen, Phys. Rev. A **90**, 055401 (2014).

[14] F. Blatt, T. Halfmann, and T. Peters, Opt. Lett. **39**, 446 (2014).

[15] K. R. Zangenberg, A. Dantan, and M. Drewsen, J. Phys. B **45**, 124011 (2012).

[16] C. Clausen, N. Sangouard, and M. Drewsen, New J. Phys. **15**, 025021 (2013).

[17] M. Sabooni, Q. Li, L. Rippe, R. K. Mohan, and S. Kröll, Phys. Rev. Lett. **111**, 183602 (2013).

[18] P. Jobez, I. Usmani, N. Timoney, C. Laplane, N. Gisin, and M. Afzelius, New J. Phys. **16**, 083005 (2014).

[19] F. Könz, Y. Sun, C. W. Thiel, R. L. Cone, R. W. Equall, R. L. Hutcheson, and R. M. Macfarlane, Phys. Rev. B **68**, 085109 (2003).

[20] F. Beaudoux, O. Guillot-Noël, J. Lejay, A. Ferrier, and P. Goldner, J. Phys. B **45**, 124014 (2012).

[21] S. Mieth, A. Henderson, and T. Halfmann, Opt. Express **22**, 11182 (2014).

[22] F. Beil, J. Klein, G. Nikoghosyan, and T. Halfmann, J. Phys. B **41**, 074001 (2008).

[23] I. Novikova, A. V. Gorshkov, D. F. Phillips, A. S. Sørensen, M. D. Lukin, and R. L. Walsworth, Phys. Rev. Lett. **98**, 243602 (2007).

[24] I. Novikova, N. B. Phillips, and A. V. Gorshkov, Phys. Rev. A **78**, 021802 (2008).